Journal of Materials Chemistry A

Chemical manipulation of phase stability and electronic behavior in Cu4-xAgxSe2

Journal:	*Journal of Materials Chemistry A*
Manuscript ID	TA-ART-02-2018-001531.R1
Article Type:	Paper
Date Submitted by the Author:	20-Mar-2018

Complete List of Authors:	Poudeu, Pierre Ferdinand; University of Michigan, Department of Materials Science and Engineering; University of Michigan, Department of Materials Science and Engineering Olvera, Alan; University of Michigan, Materials Science and Engineering Bailey, Trevor; University of Michigan, Department of Physics Uher, Ctirad; University of Michigan, Department of Physics

Chemical manipulation of phase stability and electronic behavior in $Cu_{4-x}Ag_xSe_2$

A. Olvera,[a] T.P. Bailey,[b] C. Uher,[b] P. F. P Poudeu[a,*]

[a] Laboratory for Emerging Energy and Electronic Materials, Department of Materials Science and Engineering, University of Michigan, Ann Arbor, MI, 48109, USA.

[b] Department of Physics, University of Michigan, Ann Arbor, MI, 48109, USA.

KEYWORDS: Copper, silver, chalcogenide, phase transformation, thermoelectric, composite, superionic behavior.

ABSTRACT: Superionic chalcogenides have gained renewed research interest, within the last decade, as emerging thermoelectric materials due to attractive properties such as glass-like phonon transport coupled with crystal-like carrier transport. Of particular interest has been *p*-type coinage metal-based materials (Cu_2Se, CuAgSe), which have demonstrated figures-of-merit, ZT, exceeding unity through a broad temperature range. However, the lack of *n*-type counterparts within this class of compounds limits potential module deployment. Here we show that careful stoichiometry control of the $Cu_{4-x}Ag_xSe_2$ series enables the formation of stable *n*-type materials throughout the measured temperature range upon substitution of Cu by Ag ($1 \leq x \leq 3$). Thermopower data show that the sample with x = 1 (Cu_3AgSe_2) undergoes a transition from *n*- to *p*-type conducting behavior, whereas samples with x = 2 (CuAgSe) and x = 3 ($CuAg_3Se_2$) exhibit *n*-type character in the whole measured temperature range. The post superionic transition *n*-type conductivity of CuAgSe is quite surprising and is contrary to the *n*- to *p*-type transition previously reported for this composition. Room temperature X-ray diffraction studies indicate the formation of a two-phase mixture for samples with x = 1 (Cu_3AgSe_2 = α-Cu_2Se + α-CuAgSe) and x = 3 ($CuAg_3Se_2$ = α-Ag_2Se + α-CuAgSe), whereas a single-phase α-CuAgSe is observed for the sample with x = 2. At 523 K, X-ray diffraction patterns show that Cu_3AgSe_2 (x = 1) and α-CuAgSe (x = 2) transform into single phase structure with the space group *F m-3m*, while the $CuAg_3Se_2$ (x=3) sample remains a two-phase system ($CuAg_3Se_2$ = β-Ag_2Se + β-CuAgSe) in contrast to previous studies. This structural study is consistent with the observed gradual evolution of the conduction type of $Cu_{4-x}Ag_xSe_2$ samples between the *p*-type character of Cu_2Se (x = 0) and the *n*-type semiconducting behavior for Ag_2Se (x = 4). This suggests that the conducting behavior in the $Cu_{4-x}Ag_xSe_2$ is modulated by the Cu:Ag ratio. All $Cu_{4-x}Ag_xSe_2$ samples exhibit extremely low thermal conductivity after their phase transitions (< 0.5 W $m^{-1}K^{-1}$), which result in modest ZT values (~ 0.45 at 625 K).

Introduction

Of the currently available thermoelectric (TE) materials, those most well-known for their efficiency and feasibility belong to chalcogen-based compounds, which encompass a spectrum of materials suitable for various operating conditions.[1-2] Consequently, this has motivated research efforts in the optimization of chalcogenide-based materials, including CuAgSe,[3-7] SnSe,[8-9] $Cu_{2-x}Se$,[10-15] and PbTe,[16-18] where efforts have been made to increase the material's thermoelectric figure of merit, *ZT*. For a given temperature, the *ZT* of a material dictates the conversion efficiency, where a moderate conversion efficiency can be achieved with *ZT* values greater than 1.[19] This quantity is given by the equation:

$$ZT = \frac{\sigma S^2}{\kappa_e + \kappa_L} T,$$

where σ is the electrical conductivity, *S* is the Seebeck coefficient, *T* the is absolute temperature, and κ_e and κ_L are the electronic and lattice contribution to thermal conductivity, respectively. Optimization of the figure of merit requires significant understanding of the interrelated electronic and thermal properties of a material, often making it difficult to reach high *ZT* values. However, remarkable advancements in *ZT* of new and old materials have been achieved largely due to strategic material design based on concepts spanning from band structure engineering[16, 20] and hierarchal structuring[21-22] to designing materials with complex crystal structures[23-26] or materials that behave like phonon-glass electron-crystals (PGEC).[3, 7, 27-30]

Along this line, the development of PGEC materials has flourished due to their unique properties, where reduced phonon propagation and superior carrier mobility lead to an intrinsically low κ_L and high power factor, σS^2.[31] Consequently, these materials are capable of reaching ZT values above unity. The most notable systems include $Cu_{2-\delta}M$ (M = S, Se),[14-15, 32-34] Ag_2Se,[27, 35-38] CuAgSe,[3-4, 6-7, 39] and $AgCrSe_2$.[29] For example, unoptimized Cu_2Se demonstrates a large potential in high-temperature thermoelectric modules, achieving a *ZT* of 1.5 at 1000 K, which is attributed to its PGEC behavior.[10] In this system, selenium atoms form a rigid framework that encloses a sub-lattice of structurally disordered copper ions, where the high degree of freedom in the copper sublattice ensures significant ionic mobility within the lattice.[40-41] Typically, this behavior is associated with poor electrical conductivity due to increased carrier scattering, however, this is partially mitigated by the conductive selenium framework. These unique features provide the cornerstone for performance in Cu_2Se and chemically similar compounds.[2]

While structurally distinct in their low temperature modifications, Ag_2Se and CuAgSe share similarities to Cu_2Se in that all three materials become superionic conductors above their critical transition temperature, $T_{\alpha-\beta}$. Extensive studies of the low temperature modification of Ag_2Se have demonstrated a range in figure of merit (~0.3 – 1.0) at 300 K, owing its performance to its intrinsically low thermal conductivity and relatively high electron mobility.[35-38] Above its superionic phase transition, Ag_2Se shows relatively low *ZT*,[37] but has possibilities of optimization as shown by Drymiotis *et al.*, who reported *ZT* values greater than unity at various temperatures above the superionic transition temperature.[27] A ternary analogue to Cu_2Se and Ag_2Se is CuAgSe, which hosts a superionic phase that closely resembles that of β-Cu_2Se, but with silver and copper atoms randomly distributed around tetrahedral sites enclosed by a selenium FCC framework.[42-43] Recently, CuAgSe has gained notable interest due to its unique carrier switching property, where upon transitioning from its α to β polymorph, CuAgSe shifts from *n*-type to *p*-type conducting behavior.[3-4, 7] Coupled with its intrinsically low thermal conductivity, presumably a result of highly mobile copper and silver atoms, CuAgSe is able to achieve a maximum *ZT* of 0.9 at 625 K.[3]

However, despite various emerging Cu-based superionic TE materials, there exists a lack of compatible *n*-type compounds to complement current *p*-type superionic materials in thermoelectric modules. This is particularly problematic due to possible mismatch in linear expansion coefficients that could result in premature device failure. It is therefore essential to identify potential materials with *n*-type behavior throughout a broad temperature range. Interestingly, recent investigations have suggested that CuAgSe may remain *n*-type after its superionic phase transition, attributing the *p*-type phenomenon to off-stoichiometry rather than an intrinsic behavior.[6, 39] Considering that Ag_2Se is an *n*-type material at moderate temperatures, it is anticipated that some intermediate compositions of the form $Cu_{4-x}Ag_xSe_2$ between the *p*-type Cu_2Se and the *n*-type Ag_2Se may show *n*-type behavior as well. A recent study by Asadov *et al.*, focusing on various forms of Cu- and Ag-based binary and ternary chalcogenides reported the temperature-dependent structural transformation of $Cu_{1.6}Ag_{0.4}Se$, CuAgSe, and $Cu_{0.5}Ag_{1.5}Se$.[44] In this particular study, all three compounds are found to form a high temperature superionic phase, resembling β-Cu_2Se. Given the intriguing thermal and electronic properties of β-Cu_2Se and the lack of high temperature electronic characterization of the $Cu_{4-x}Ag_xSe_2$ system of materials, we have initiated this study to investigate the effects of Cu:Ag ratio on the phase stability and thermoelectric behavior of three compositions in the $Cu_{4-x}Ag_xSe_2$ system, namely x = 1, 2, and 3.

Experimental details

Synthesis. Polycrystalline powders of Cu_3AgSe_2 (x = 1), CuAgSe (x = 2), and $CuAg_3Se_2$ (x = 3) were synthesized via planetary ball milling of stoichiometric amounts of elemental powder of Cu (Sigma Aldrich, 99.99%), Ag (Sigma Aldrich, 99.99%), and Se (Sigma Aldrich, 99.5%+). Powder preparation was carried out in an argon-filled glove box, where the stoichiometric mixtures were loaded into agate jars containing agate milling balls at a 5:1 ball-to-sample mass ratio. The jars were sealed in an argon glove box to minimize oxygen contamination during the milling process. The sealed

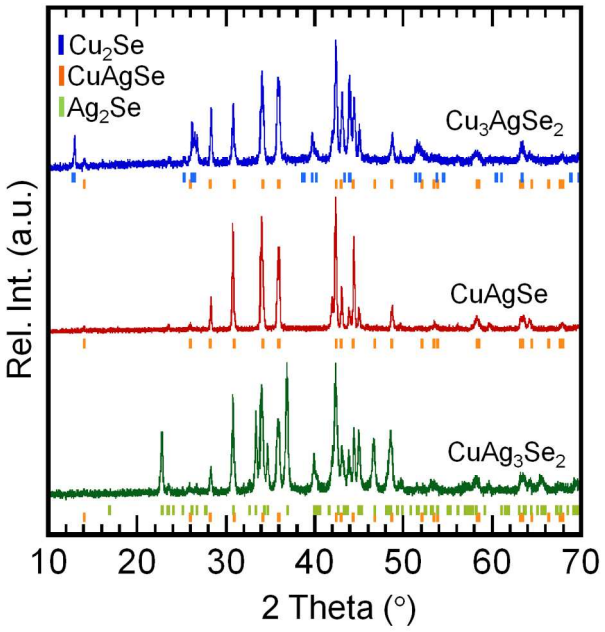

Figure 1: Powder X-ray diffraction patterns of $Cu_{4-x}Ag_xSe_2$ samples at 300 K. Theoretical patterns of Cu_2Se, CuAgSe, and Ag_2Se are denoted by the blue, orange and green vertical lines, respectively.

planetary ball mill (Across International, PQ-N2) and mechanically alloyed for 16 hours with spin rotation reversed every 4 hours. This process resulted in extra-fine black powders that were consolidated *via* spark plasma sintering at 873 K and 50 MPa for 10 minutes. Pellet density (ρ) was measured by helium pycnometry using a Quantachrome micro Ultrapyc 1200e.

X-ray diffraction (XRD). Structure and phase identification was completed using temperature-dependent X-ray diffraction data collected on a Rigaku Ultima X-ray diffractometer equipped with graphite monochromated Cu Kα radiation operating at 40 kV and 100 mA. XRD patterns were taken on sintered pellets using a step size of 0.01 and time-per-step of ~ 0.51 s / step.

Thermal characterization. Thermal diffusivity (D) was measured from room temperature to 623 K *via* the laser flash method using a Linseis LFA 1000. Heat capacity (C_p) was measured using a Netzch DSC 404F1 Pegasus, where C_p was calculated using the ratio method and a certified sapphire reference. Thermal conductivity was calculated from the equation $\kappa = C_p \times D \times \rho$.

Electronic property characterization. Electrical conductivity (σ) and Seebeck coefficient (S) were measured simultaneously using a commercially available apparatus (ZEM-3, ULVAC-RIKO). Rectangular sample bars were cut from densified pellets and measured under partial helium pressure from room temperature to 623 K.

Hall effect. Hall effect measurements were performed using an AC 4-probe method in a custom built apparatus under a maximum field of 1 Tesla. The carrier concentration (n) and mobility (μ) were extracted using the Hall coefficient ($R_H = (n \times e)^{-1}$) and the electrical conductivity data ($\sigma = ne\mu$), respectively.

Phase morphology. The microstructure and chemical composition of sintered samples were characterized with the aid of scanning electron microscopy (SEM) and energy dispersive spectroscopy (EDS) using a JEOL-7800FLV FE SEM equipped with an Oxford EDAX system.

Results and discussion

Structural and morphological characterization.

Analysis of room temperature X-ray diffraction patterns for Cu_3AgSe_2 (x = 1), CuAgSe (x = 2), and $CuAg_3Se_2$ (x = 3) show that each composition can be indexed with a combination of tetragonal CuAgSe, monoclinic Cu_2Se, and/or orthorhombic Ag_2Se (**Figure 1**). These results are consistent with previous studies.[44-45] However, careful examination of all XRD pattern shows additional Bragg peaks not accounted for by tetragonal CuAgSe. This discrepancy has been noted in previous studies and has been identified as orthorhombic CuAgSe, which coexists with tetragonal CuAgSe.[46] Using the orthorhombic crystal structure for CuAgSe, the additional Bragg peaks can be properly indexed, suggesting single-phase CuAgSe (**Figure S1**). It is important to note that while Cu_2Se and Ag_2Se have been shown to allow partial solubility of Ag and Cu, respectively, CuAgSe has a relatively strict intolerance for off-stoichiometry at 300K. In fact, it has been shown that a small excess or deficiency of Cu, Ag, and/or Se results in phase segregation with the exception being that CuAgSe can tolerate a small amount of Ag deficiency.[6] Depending on the degree of off-stoichiometry, a nominal composition of CuAgSe will additionally consist of Ag_2Se and/or Cu_2Se.

Given the strict stoichiometric adherence of CuAgSe, it is expected that the Cu_3AgSe_2 and $CuAg_3Se_2$ samples, which form a two-phase mixture, will show relatively distinct phase boundaries between the coexisting ternary phase (CuAgSe) and the binary phases (Cu_2Se, Ag_2Se). Backscatter scanning electron microscopy images and composition mapping of Cu_3AgSe_2 show somewhat obscure phase boundaries between the Ag-rich regions, CuAgSe, and the Cu-rich regions, Cu_2Se (**Figure 2A**). In contrast, CuAgSe shows a homogenous phase, where elemental mapping shows no signature of impurity binary phases (**Figure 2B**) and is in agreement with XRD analysis. Lastly, Cu_3AgSe_2 shows distinct phase boundaries between the Cu-rich phase, CuAgSe, and the Ag-rich phase, Ag_2Se (**Figure 2C**). This may suggest that CuAgSe and Ag_2Se are not fully miscible at high temperatures, but instead remain as two separate phases. Interestingly, there are noticeable copper channels appearing between larger islands of Ag_2Se, presumably a result of the high mobility of copper ions within Ag_2Se.

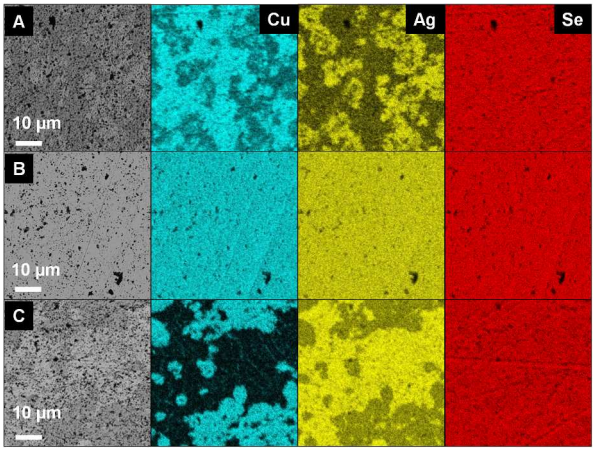

Figure 2: Scanning electron microscopy images of selected $Cu_{4-x}Ag_xSe_2$ samples showing backscatter electron micrographs and their corresponding electron dispersive spectroscopy mapping for copper, silver, and selenium. Each row is represented by the compositions A) Cu_3AgSe_2 (x = 1), B) CuAgSe (x = 2), and C) $CuAg_3Se_2$ (x = 3).

To further understand the structural relationships between the room temperature and high temperature modifications of Cu_3AgSe_2 (x = 1), CuAgSe (x = 2), and $CuAg_3Se_2$ (x = 3), high temperature X-ray diffraction patterns were collected on all three samples. **Figure 3A** shows XRD patterns taken at 403 K and 433 K for samples with x = 1 (Cu_3AgSe_2) and x = 3 ($CuAg_3Se_2$), respectively. These temperatures were selected based on heat capacity data (**Figure 3C**), which correspond to the superionic phase transitions of Cu_2Se and Ag_2Se at approximately 380 K and 390 K, respectively. These transition temperatures are consistent with previously reported values for pristine Cu_2Se and Ag_2Se phases.[47-48] Analysis of XRD patterns for x = 1 and x = 3 samples indicate that at the measured temperatures, Cu_2Se and Ag_2Se have transformed into their superionic β-phase, while the CuAgSe components remain in the α-phase. Following the α-β transitions in Cu_3AgSe_2 and $CuAg_3Se_2$, heat capacity data show a gradual increase in magnitude until the secondary thermal event, which occurs at ~ 440 K and ~ 467 K for Cu_3AgSe_2 and $CuAg_3Se_2$, respectively. For x = 1, The increase in C_p between 390 - 440 K suggests that there is a partial dissolution of CuAgSe into Cu_2Se, which has been not-

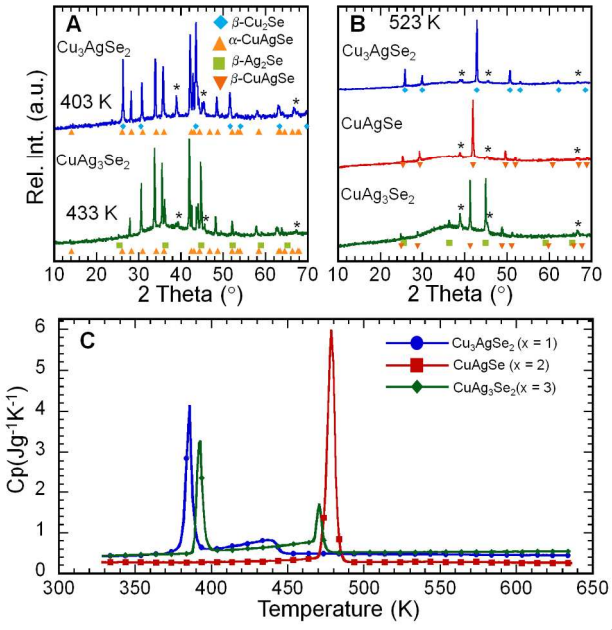

Figure 3: Structural and thermal characterization of $Cu_{4-x}Ag_xSe_2$ samples. Temperature-dependent X-ray diffraction at A) 403 K and 423 K; and B) 523 K showing intermediate and final phase transformations in various samples. Diffraction temperature were taken according to thermal events observed in C) specific heat capacity measurements. Peaks marked by an asterisk (*) belong to the platinum holder (Figure S2).

ed to occur in Cu_2Se-CuAgSe mixtures.[49]. Given the gradual dissolution of CuAgSe into Cu_2Se, as indicated by C_p measurements, it becomes evident that the comparably diffuse interfaces between Cu_2Se and CuAgSe in **Figure 2A** are a result of the gradual transition from one phase to another as the material cooled from the high-temperature sintering conditions. Similarly, x = 3 shows increasing C_p from 400 – 465 K that is likely due to the dissolution of one phase into the other.

As shown in **Figure 3B**, X-ray diffraction patterns at 523 K suggest that Cu_3AgSe_2 and CuAgSe have transformed into single-phase materials. Further analysis of XRD patterns indicates that both materials can be structurally refined with the space group *Fm-3m*, where the lattice parameters for Cu_3AgSe_2 and CuAgSe are 5.97 Å and 6.09 Å, respectively (Figures S3 and S4). When compared to pure Cu_2Se (a =5. 787 at 433 K),[50] it is clear that Ag has fully incorporated into the Cu_2Se structure type. Alternatively, the high temperature lattice parameter of CuAgSe matches with existing literature, which further confirms the phase purity of the synthesized CuAgSe.[46] For $CuAg_3Se_2$, XRD refinement shows that all peaks can be indexed to β-CuAgSe and β-Ag_2Se (Figure S5). This finding is in contrast to previous studies that reported that the composition $CuAg_3Se_2$ becomes single phase at high temperatures.[44] Similarly, the coexistence of two cubic phases at high temperature in the $CuAg_3Se_2$ sample explains why EDS mapping of the sintered pellet at room temperature shows large distinct phases of α-Ag_2Se and α-CuAgSe with sharp phase boundaries (**Figure 2C**). Lattice parameter refinement of $CuAg_3Se_2$ shows that CuAgSe (a = 6.18 Å) in this two-phase system has a greater lattice parameter than what was found for CuAgSe (a = 6.09 Å). This suggests that β-CuAgSe has a greater capability to accommodate a significant amount of excess silver, something that is not true for room temperature α-CuAgSe.[6] Therefore, it is possible that non-stoichiometric CuAgSe may be responsible for the discrepancies in reported electronic transport properties.

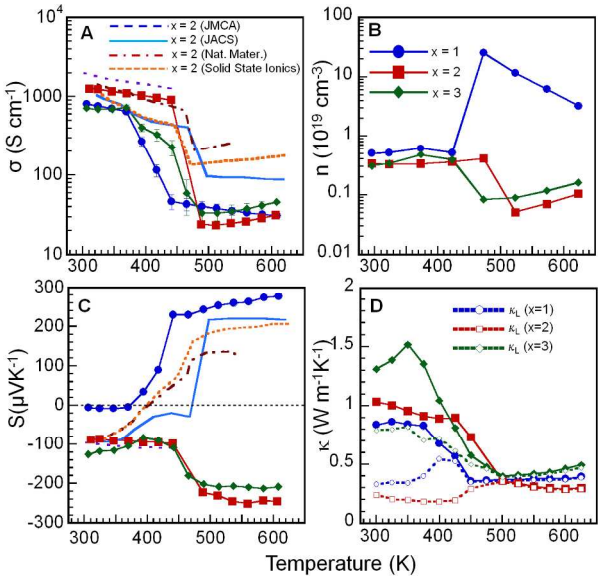

Figure 4 Electronic and thermal transport properties of $Cu_{4-x}Ag_xSe_2$. **A)** electrical conductivity, **B)** carrier concentration, **C)** Seebeck coefficient, and **D)** total and lattice thermal conductivity for Cu_3AgSe_2, CuAgSe, and $CuAg_3Se_2$ samples. Reported values of the electrical conductivity and Seebeck coefficient for CuAgSe shown for comparison and discussion of the effect non-stoichiometry may have on its electronic properties.[3-4, 6-7]

Electronic transport. All materials show relatively high electrical conductivity, with room temperature values ranging from approximately 715 S/cm for the samples with x = 1 and x = 3 to 1280 S/cm for CuAgSe (x = 2) (**Figure 4A**). The observed room temperature value of the electrical conductivity for stoichiometric CuAgSe is slightly lower than previously reported values,[6] but this is likely attributed to increased carrier scattering at multiple grain boundary interfaces resulting from the ball milling procedure. Electrical conductivity slightly decreases as all materials approach their corresponding phase transitions and is followed by a sharp drop by at least an order of magnitude after all materials have reached their superionic high temperature cubic structures. The large decrease in the electrical conductivity is partially attributed to the highly dynamic superionic phases of each material. The increased mobility of Cu and Ag ions within the β-phases drastically increases carrier scattering, leading to a decrease in carrier mobility (**Figure 5A**). This effect is particularly strong for Cu_3AgSe_2, in which the extremely poor carrier mobility above the phase transition shadows the large increase in carrier concentration **(Figure 4B).** However, the reduction in electrical conductivity for CuAgSe and $CuAg_3Se_2$ is largely due to a decrease in carrier concentration given the marginal drop in the carrier mobility.

For all materials, absolute Seebeck coefficient of all materials is inversely proportional to electrical conductivity (**Figure 4C**). Additionally, all materials show negative values of the Seebeck coefficient at low temperatures ($T < T_{\alpha-\beta}$), indicating *n*-type behavior. This is further supported by Hall coefficient measurements (**Figure 5B**). However, at temperatures above the final phase transition of each composition, the Seebeck coefficient changes considerably. Cu_3AgSe_2 undergoes a transition from *n*-type to *p*-type semiconducting behavior, whereas the compositions with CuAgSe and $CuAg_3Se_2$ remain *n*-type. With respect to Cu_3AgSe_2, the near-zero negative value of the Seebeck coefficient measured at temperatures below $T_{\alpha-\beta,\ Cu_2Se}$ is a result of the individual *n*- and *p*-type behavior of CuAgSe and Cu_2Se, respectively. As the α-Cu_2Se transitions into its superionic β-phase near 380 K, the total Seebeck coefficient switches to *p*-type and continues to grow *p*-type even after Cu_3AgSe_2 becomes a single-phase superionic

compound at T ~ 440 K (**Figure 4C**). At this point, the Seebeck coefficient monotonically increases as a function of temperature partly due to the decrease in carrier concentration (**Figure 4B**). This behavior is expected according to

$$S = \frac{k}{e}\left(A + ln\frac{2(2\pi m^* kT)^{\frac{3}{2}}}{h^3 n}\right),$$

where S is the Seebeck coefficient, A is the carrier scattering parameter, m^* is the effective mass, and n is the carrier concentration. However, this relation only applies to compositions that are single phase and therefore, excludes the behavior of Cu_3AgSe_2 below 440K and the behavior of the $CuAg_3Se_2$ sample over the entire measured temperature range.

In the case of CuAgSe, the Seebeck coefficient around 300 K agrees well with recent studies.[6, 39] However, it differs significantly near the α-β phase transition temperature ($T_{\alpha-\beta,CuAgSe}$ ~ 470 K). For instance, previous studies show that CuAgSe transitions from *n*-type to *p*-type as the temperature approaches its superionic phase transition (**Figure 4C**).[3-4, 7] However, the validity of this *n*-*p* transition for chemically stoichiometric CuAgSe has been put in question due to evidence showing that stoichiometric defects dominate transport properties in CuAgSe above room temperature, where Ag or Cu deficiencies act as significant *p*-type dopants.[6] According to the Seebeck relation described above, pristine CuAgSe should show a nearly linear increase in absolute Seebeck coefficient as a function of temperature assuming all other factors remain constant, which is consistent with our experimental data observed below 470 K (**Figure 4C**). Above 470 K, the Seebeck coefficient of CuAgSe becomes increasingly negative, showing a change from -100 μV/K to -220 μV/K. This demonstrates that CuAgSe is an *n*-type semiconductor above its superionic phase transition, which is further supported by the negative Hall coefficient throughout the measured temperature range (**Figure 5B).** Therefore, one can derive that the *p*-type behavior often observed for CuAgSe in previous studies presumably arises from a combination of the presence of Cu or Ag deficiencies which lead to heavy hole doping of an otherwise *n*-type semiconductor. In the present study, the lack of Cu and Ag deficiencies in the synthesized CuAgSe phase explains why the system remains *n*-type after the transition to the superionic cubic β-phase. Holes created by the disordered Cu, Ag ions above the transition only partially compensate conducting electrons within the CuAgSe matrix, leading to the observed marginal decrease in the overall electron density and large increase in the Seebeck coefficient above the transition (**Figures 4B, 4C**). Therefore, stoichiometric control is required for CuAgSe to remain *n*-type after its superionic transition. This makes CuAgSe a unique copper chalcogenide in that it can exhibit *n*-type and *p*-type behavior at high temperatures.

In the case of $CuAg_3Se_2$, the total Seebeck coefficient can be described as the weighted sum of both components in Cu_3AgSe_2, namely α-Ag_2Se and α-CuAgSe. Below ~ 470 K, the Seebeck coefficient is larger than that of α-CuAgSe due to the contribution from α-Ag_2Se, but as both components reach their β-phases, CuAgSe contributes more to the overall Seebeck coefficient. From the above results, the overall conduction type in $Cu_{4-x}Ag_xSe_2$ (x = 1, 2, 3) materials evolve from the *p*-type character measured in Cu_2Se (x = 0) to the robust *n*-type behavior in CuAgSe (x = 2) suggesting that the incorporation of silver in the structure of Cu_2Se moves the Fermi energy near to the conduction band edge.

Thermal conductivity. Based on the analysis above, the thermal conductivity of each composition can be adequately described. For example, at low temperatures (T < 440 K) the composition of Cu_3AgSe_2 consists of two relatively large lattices with low symmetry. This makes it likely that the overall composition will have poor lattice thermal conductivity and suggests that the majority of thermal energy may be transported *via* electronic carriers. To confirm this analysis, the electronic contribution (κ_e) to the thermal conductivity was estimated using the Wiedemann-Franz law: $\kappa_e = \sigma LT$, where the L is the Lorenz number. For degenerate semiconductors, the value of the Lorenz number is typically assumed to be 2.44 x 10^{-8} $W\Omega K^{-2}$, but at intermediate carrier concentrations using this value of the Lorenz number may result in large errors when calculating κ_e. Assuming that all compositions behave according to the single parabolic band model and are dominated by acoustic phonon scattering, the Lorenz number can be approximated by the equation:

$$L = 1.5 + \exp\left[-\frac{|S|}{116}\right],$$

where L is in units of 10^{-8} $W\Omega K^{-2}$ and S in μV/K. However, it is critical to note that the calculation of κ_e and consequently the lattice thermal conductivity (κ_L) is only an approximation and should be treated accordingly.[51] **Figure 4D** shows the total thermal conductivity (κ_T) of all compositions. At 300 K, $CuAg_3Se_2$ exhibits the highest κ_T of all three compositions (κ_T = 1.4 W $m^{-1}K^{-1}$), while Cu_3AgSe_2 shows the lowest κ_T (κ_T = 0.9 W $m^{-1}K^{-1}$) with an intermediate value observed for CuAgSe (κ_T = 1.0 W $m^{-1}K^{-1}$). At temperatures below the respective superionic transitions, the total thermal conductivity of the Cu_3AgSe_2 and $CuAg_3Se_2$ samples is a combination of the total thermal conductivity of the two coexisting phases. For Cu_3AgSe_2, the total thermal conductivity is largely dominated by the contribution

from α-CuAgSe below 380 K, due to its large electrical conductivity. However, as the temperature approaches the transition point, the electrical conductivity plummets and κ_T becomes almost entirely associated with the lattice contribution. Between 450 K and 625 K, Cu_3AgSe_2 shows a slight increase from 0.31 W $m^{-1}K^{-1}$ to 0.39 W $m^{-1}K^{-1}$. Similarly, at low temperatures CuAgSe is dominated by κ_e, but as the temperature surpasses 470 K, the total thermal conductivity is essentially identical to the lattice contribution and continues to decrease from 0.35 W $m^{-1}K^{-1}$ at 470 K to 0.29 W $m^{-1}K^{-1}$ at 625 K. Lastly, $CuAg_3Se_2$ shows a moderate contribution from κ_L and κ_e. As was observed for the other two compositions, the total thermal conductivity after the final phase transition consists mostly of the lattice contribution and shows a slight upward trend from 0.40 W $m^{-1}K^{-1}$ to 0.46 W $m^{-1}K^{-1}$ at 500 K and 625 K, respectively.

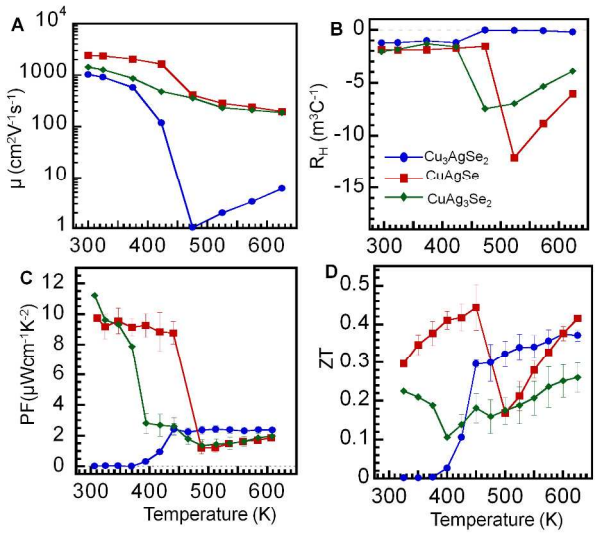

Figure 5: Temperature-dependent (A) Hall mobility, (B) Hall coefficient, (C) Power Factor (PF) and (D) Figure of merit, ZT, of $Cu_{4-x}Ag_xSe_2$.

Power factor and ZT. At temperatures below 470 K, the power factor for various samples shows unique trends that are consistent with the observed phase transformations (**Figure 5C**). For instance, the power factor for the Cu_3AgSe_2 sample at temperatures below $T_{\alpha-\beta,\ Cu_2Se}$ is nearly zero due to the low Seebeck coefficient and remains relatively constant from 300 K to 375 K. However, at 390K a sharp increase in the power factor occurs, increasing to ~2.5 μWcm^{-1}K^{-2} at 440 K and remaining relatively constant up to 625 K. This modest PF coupled with ultra-low thermal conductivity at temperatures above 390 K results in ZT values as high as 0.37 at 625 K (**Figure 5D**). While not a remarkable figure of merit, the trend in Seebeck coefficient and thermal conductivity at temperatures greater than 470 K show a promising avenue for the optimization of the thermoelectric behavior of Cu_3AgSe_2. Alternatively, CuAgSe provides an interesting opportunity for integration into thermoelectric devices due to its relatively stable power factor and thermal conductivity before and after its α-β transition. At temperatures below $T_{\alpha-\beta,\ CuAgSe}$, ZT reaches a value of ~ 0.45 at 450 K. This is followed by an abrupt decrease to ~ 0.19 at 500 K due to the phase transformation. However, the ZT quickly increases, reaching a maximum of 0.42 at 625 K. As was mentioned for Cu_3AgSe_2, at temperatures greater than 470 K, the gradual increase in the absolute Seebeck coefficient coupled with low thermal conductivity makes it possible to increase ZT *via* carrier concentration optimization. However, an even more interesting prospect is that the present results indicate that CuAgSe exists as *n*-type at high temperatures, making it possible to create a thermoelectric module consisting of *n*-type and *p*-type CuAgSe. Of the three compositions, $CuAg_3Se_2$ remains as a two-component system throughout the measured temperature range, despite previous reports claiming it becomes a single phase similar in structure to that of Cu_3AgSe_2 and CuAgSe. The power factor deteriorates as Cu_3AgSe_2 crosses its final transition temperature at about 470 K, but closely follows the same value and trend as CuAgSe from 475 K to 625 K. Despite this comparable power factor, the relatively high thermal conductivity of $CuAg_3Se_2$ results in a maximum ZT of ~0.26 at 625 K. Unfortunately, the inability to become single phase at high temperatures limits the possibility of ZT optimization in Cu_3AgSe_2.

Conclusion

In summary, several samples in the $Cu_{4-x}Ag_xSe_2$ system (x = 1, 2, 3) were synthesized in order to investigate the effect of chemical composition (Cu:Ag ratio) on their structural stability and thermoelectric performance at various temperatures. It was found that the samples with x = 1 (Cu_3AgSe_2) and x = 3 ($CuAg_3Se_2$), decompose into a two-phase composite at low temperatures (T < 470K), which is consistent with previous reports on this material system. However, at high temperatures (T > 470K), the coexisting phases in Cu_3AgSe_2 (α-Cu_2Se and α-CuAgSe) combine into a single phase, whereas coexisting phases in $CuAg_3Se_2$ (α-Ag_2Se and α-CuAgSe) remain phase separated and transform into their respective β-phases. The inability to become single-phase makes $CuAg_3Se_2$ a complex composite with little possibility for thermoelectric optimization. Two important results can be derived from this study. First, the confirmation of Cu_3AgSe_2 as a single-phase structure at high temperatures provides a broad avenue for thermoelectric optimization given its low thermal conductivity and potentially tunable carrier concentra-

tion. A major drawback is that potential TE modules based on this material must operate above 470 K, which may limit its usefulness. However, additional work must be done to verify if single-phase Cu_3AgSe_2 can be stabilized within a broader temperature range, e.g., by sulfur to selenium substitution. The second important result of this work is the demonstration of CuAgSe as a stable *n*-type material above its superionic transition temperature. This verifies that while off-stoichiometric compositions of CuAgSe exist as a single-phase, the nature of their defects dramatically change the resulting electronic properties.

AUTHOR INFORMATION

Corresponding Author

* Correspondence to: ppoudeup@umich.edu

Author Contributions

A.O. synthesized the samples, carried out structural characterization, performed the SEM characterization, performed high temperature electronic and thermal conductivity measurements, performed data analysis, and co-wrote the manuscript. T.P.B. and C.U. performed high temperature Hall effect, electrical conductivity and Seebeck coefficient measurements and co-edited the manuscript. P.F.P.P. conceived the experiment, performed data analysis and co-wrote the manuscript.

Notes

The authors declare no competing financial interest.

ACKNOWLEDGMENT

We gratefully acknowledge the financial support from the Department of Energy, Office of Basic Energy Science under Award # DE-SC-0008574 for measurement of the thermoelectric properties. Materials synthesis and structural characterization were supported by the National Science Foundation through grant number DMR 1561008. We also thank the generous gift from Kendall and Susan Warren to the UM College of Engineering in support of research in renewable energy generation. This work also made use of the SEMs (FEI Quanta3D and FEI Nova Nanolab) from the Michigan Materials Characterization Center, $(MC)^2$, purchased with funds from the National Science Foundation Awards DMR-0315633 and DMR-0723032.

REFERENCES

1 G. J. Snyder and E. S. Toberer, *Nat Mater* 2008, **7**, 105-114.
2 P. Qiu, X. Shi and L. Chen, *Energy Storage Materials* 2016, **3**, 85-97.
3 A. J. Hong, L. Li, H. X. Zhu, X. H. Zhou, Q. Y. He, W. S. Liu, Z. B. Yan, J. M. Liu and Z. F. Ren, *Solid State Ionics* 2014, **261**, 21-25.
4 S. Ishiwata, Y. Shiomi, J. S. Lee, M. S. Bahramy, T. Suzuki, M. Uchida, R. Arita, Y. Taguchi and Y. Tokura, *Nat Mater* 2013, **12**, 512-517.
5 N. Moroz, A. Olvera, G. Willis and P. F. Poudeu, *Nanoscale* 2015.
6 X. Wang, P. Qiu, T. Zhang, D. Ren, L. Wu, X. Shi, J. Yang and L. Chen, *J. Mater. Chem. A* 2015, **3**, 13662-13670.
7 C. Han, Q. Sun, Z. X. Cheng, J. L. Wang, Z. Li, G. Q. Lu and S. X. Dou, *J Am Chem Soc* 2014, **136**, 17626-17633.
8 L. D. Zhao, G. J. Tan, S. Q. Hao, J. Q. He, Y. L. Pei, H. Chi, H. Wang, S. K. Gong, H. B. Xu, V. P. Dravid, C. Uher, G. J. Snyder, C. Wolverton and M. G. Kanatzidis, *Science* 2016, **351**, 141-144.
9 L. D. Zhao, S. H. Lo, Y. S. Zhang, H. Sun, G. J. Tan, C. Uher, C. Wolverton, V. P. Dravid and M. G. Kanatzidis, *Nature* 2014, **508**, 373-+.
10 H. L. Liu, X. Shi, F. F. Xu, L. L. Zhang, W. Q. Zhang, L. D. Chen, Q. Li, C. Uher, T. Day and G. J. Snyder, *Nature Materials* 2012, **11**, 422-425.
11 F. S. Liu, M. J. Huang, Z. N. Gong, W. Q. Ao, Y. Li and J. Q. Li, *Journal of Alloys and Compounds* 2015, **651**, 648-654.
12 L. Yang, Z.-G. Chen, G. Han, M. Hong, Y. Zou and J. Zou, *Nano Energy* 2015, **16**, 367-374.
13 G. B. Abdullaezv, A. Aliyarova An and G. A. Asadov, *physica status solidi* 1967, **21**, 461.
14 T. P. Bailey, S. Hui, H. Xie, A. Olvera, P. F. P. Poudeu, X. Tang and C. Uher, *Journal of Materials Chemistry A* 2016, **4**, 17225-17235.
15 A. Olvera, N. Moroz, P. Sahoo, P. Ren, T. Bailey, A. Page, C. Uher and P. F. Poudeu, *Energy & Environmental Science* 2017, **10**, 1668.
16 J. P. Heremans, V. Jovovic, E. S. Toberer, A. Saramat, K. Kurosaki, A. Charoenphakdee, S. Yamanaka and G. J. Snyder, *Science* 2008, **321**, 554-557.
17 J. R. Sootsman, H. Kong, C. Uher, J. J. D'Angelo, C. I. Wu, T. P. Hogan, T. Caillat and M. G. Kanatzidis, *Angew Chem Int Ed Engl* 2008, **47**, 8618-8622.
18 Y. Pei, Z. M. Gibbs, A. Gloskovskii, B. Balke, W. G. Zeier and G. J. Snyder, *Advanced Energy Materials* 2014, **4**, 1400486.
19 X. Zhang and L.-D. Zhao, *Journal of Materiomics* 2015, **1**, 92-105.
20 Y. Pei, X. Shi, A. LaLonde, H. Wang, L. Chen and G. J. Snyder, *Nature* 2011, **473**, 66-69.
21 L.-D. Zhao, S. Hao, S.-H. Lo, C.-I. Wu, X. Zhou, Y. Lee, H. Li, K. Biswas, T. P. Hogan, C. Uher, C. Wolverton, V. P. Dravid and M. G. Kanatzidis, *Journal of the American Chemical Society* 2013, **135**, 7364-7370.
22 K. Biswas, J. He, I. D. Blum, C.-I. Wu, T. P. Hogan, D. N. Seidman, V. P. Dravid and M. G. Kanatzidis, *Nature* 2012, **489**, 414-418.
23 S. Q. Bai, Y. Z. Pei, L. D. Chen, W. Q. Zhang, X. Y. Zhao and J. Yang, *Acta Materialia* 2009, **57**, 3135-3139.
24 G. Rogl, A. Grytsiv, K. Yubuta, S. Puchegger, E. Bauer, C. Raju, R. C. Mallik and P. Rogl, *Acta Materialia* 2015, **95**, 201-211.
25 X. Shi, J. Yang, J. R. Salvador, M. Chi, J. Y. Cho, H. Wang, S. Bai, J. Yang, W. Zhang and L. Chen, *Journal of the American Chemical Society* 2011, **133**, 7837-7846.
26 A. Olvera, G. Shi, H. Djieutedjeu, A. Page, C. Uher, E. Kioupakis and P. F. P. Poudeu, *Inorganic Chemistry* 2015, **54**, 746-755.
27 F. Drymiotis, T. W. Day, D. R. Brown, N. A. Heinz and G. J. Snyder, *Applied Physics Letters* 2013, **103**, 143906.
28 P. Qiu, T. Zhang, Y. Qiu, X. Shi and L. Chen, *Energy & Environmental Science* 2014, **7**, 4000-4006.
29 F. Gascoin and A. Maignan, *Chemistry of Materials* 2011, **23**, 2510-2513.
30 K. S. Weldert, W. G. Zeier, T. W. Day, M. Panthofer, G. J. Snyder and W. Tremel, *J Am Chem Soc* 2014, **136**, 12035-12040.
31 A. S. Glen in *New Materials and Performance Limits for Thermoelectric Cooling*, *Vol.* CRC Press, **1995**.

32 H. Liu, X. Shi, F. Xu, L. Zhang, W. Zhang, L. Chen, Q. Li, C. Uher, T. Day and G. J. Snyder, *Nat Mater* 2012, **11**, 422-425.

33 H. L. Liu, X. Yuan, P. Lu, X. Shi, F. F. Xu, Y. He, Y. S. Tang, S. Q. Bai, W. Q. Zhang, L. D. Chen, Y. Lin, L. Shi, H. Lin, X. Y. Gao, X. M. Zhang, H. Chi and C. Uher, *Advanced Materials* 2013, **25**, 6607-6612.

34 Y. He, T. Day, T. Zhang, H. Liu, X. Shi, L. Chen and G. J. Snyder, *Advanced Materials* 2014, **26**, 3974-3978.

35 M. Ferhat and J. Nagao, *Journal of Applied Physics* 2000, **88**, 813-816.

36 F. F. Aliev, M. B. Jafarov and V. I. Eminova, *Semiconductors* 2009, **43**, 977-979.

37 W. Mi, P. Qiu, T. Zhang, Y. Lv, X. Shi and L. Chen, *Applied Physics Letters* 2014, **104**, 133903.

38 H. Z. Duan, Y. L. Li, K. P. Zhao, P. F. Qiu, X. Shi and L. D. Chen, *JOM* 2016, **68**, 2659-2665.

39 P. F. Qiu, X. B. Wang, T. S. Zhang, X. Shi and L. D. Chen, *Journal of Materials Chemistry A* 2015, **3**, 22454-22461.

40 H. Kim, S. Ballikaya, H. Chi, J.-P. Ahn, K. Ahn, C. Uher and M. Kaviany, *Acta Materialia* 2015, **86**, 247-253.

41 M. Horvatic and Z. Vucic, *Solid State Ionics* 1984, **13**, 117-125.

42 C. Shi, X. Xi, Z. Hou, E. Liu, W. Wang, S. Jin, Y. Wu and G. Wu, *The Journal of Physical Chemistry C* 2016, **120**, 3229-3234.

43 K. Basar, T. Shimoyama, D. Hosaka, XiangLian, T. Sakuma and M. Arai, *Journal of Thermal Analysis and Calorimetry* 2005, **81**, 507-510.

44 Y. G. Asadov, Y. I. Aliyev and A. G. Babaev, *Physics of Particles and Nuclei* 2015, **46**, 452-474.

45 K. Kiazimov, K. M. Jafarov and Y. G. Asadov, *Phase Transitions* 1990, **21**, 11-21.

46 R. B. Baikulov and Y. G. Asadov, *Inorganic Materials* 2005, **41**, 338-342.

47 L. Gulay, Daszkiewicz, M., Strok, O. & Pietraszko, A., *Chemistry of Metals and Alloys* 2011, **4**, 200–205

48 C. Xiao, J. Xu, K. Li, J. Feng, J. Yang and Y. Xie, *J Am Chem Soc* 2012, **134**, 4287-4293.

49 T. W. Day, K. A. Borup, T. Zhang, F. Drymiotis, D. R. Brown, X. Shi, L. Chen, B. B. Iversen and G. J. Snyder, *Materials for Renewable and Sustainable Energy* 2014, **3**, 26.

50 K. Yamamoto and S. Kashida, *Journal of Solid State Chemistry* 1991, **93**, 202-211.

51 H.-S. Kim, Z. M. Gibbs, Y. Tang, H. Wang and G. J. Snyder, *APL Materials* 2015, **3**, 041506.

Table of Contents artwork

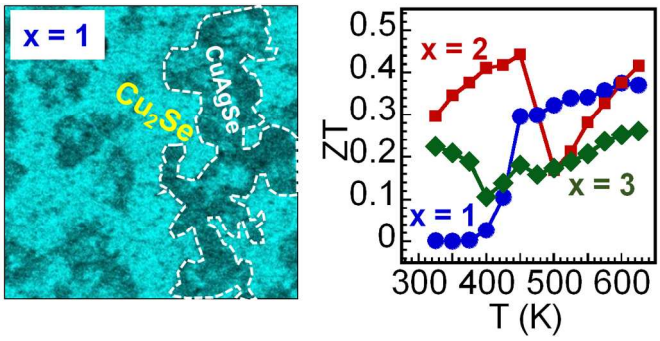

Gradual stoechiometric chemical substitution of Cu by Ag in the p-type Cu2Se phase enable phase segregation and incremental switching of the electronic transport to n-type behavior for large Ag/Cu ratios

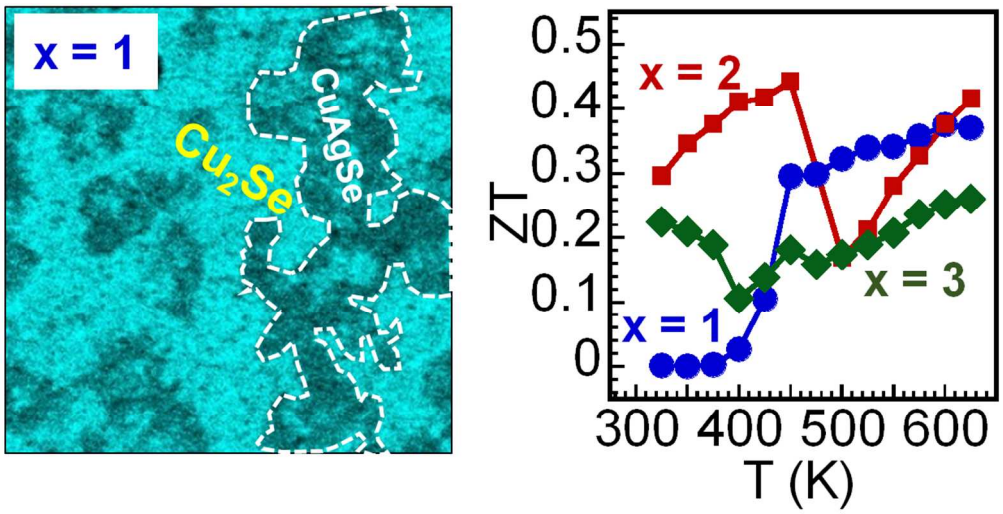

136x70mm (230 x 230 DPI)